Relativistic coupled-cluster analysis of the second-order effects on the hyperfine structure in ^{133}Cs

Fei-Chen Li [1,2] and Yong-Bo Tang [1,*]

^{1}*Physics Teaching and Experiment Center, Shenzhen Technology University, Shenzhen 518118, China*
^{2}*Department of Physics, Henan University of Technology, Zhengzhou 450001, China*

Using the single and double approximated relativistic coupled-cluster method, we calculate the first-order hyperfine structure constants for the $6p_{3/2}$, $8p_{3/2}$, $6d_{3/2}$, $7d_{3/2}$, and $7d_{5/2}$ states in ^{133}Cs, and also evaluate the second-order magnetic dipole–magnetic dipole, magnetic dipole–electric quadrupole effects caused by the off-diagonal hyperfine interaction. With these calculations, we reanalyze some recent high-precision experimental measurements of the hyperfine splitting intervals of ^{133}Cs. We find that the second-order magnetic dipole–magnetic dipole effects are especially sizable at the order of kHz in the B constant for the $d_{3/2,5/2}$ states. Our calculations can provide a reference for future higher precision experimental measurements.

I. INTRODUCTION

The atomic hyperfine structure (HFS) arises from the electron-nucleus interaction, which is thus sensitive to the properties of the nucleus and to the electronic wave functions in the nuclear region [1]. Comparison of measured and calculated values of the HFS provides information about nuclear as well as electronic structures. Such hyperfine comparison also plays a critical role in atomic parity violation (APV) studies, which is basically a process of evaluating the uncertainty of theoretical parity nonconserved amplitude [2].

High-precision experimental and theoretical studies on the HFS of atomic cesium have attracted continuous attention because the simple electronic structure containing a single valence electron makes calculations easier and the high atomic number leads to an enhanced APV effect [3–7]. In recent years, the measurement accuracy of hyperfine splittings in several states of cesium has reached a very high level of about tens to a few kHz (see Ref. [8] for these measurements). This is not only sufficient to extract the magnetic dipole ($M1$) HFS constant A, but also supports the evaluation of the electric quadrupole ($E2$) HFS constant B, and can even give nonzero magnetic octupole ($M3$) HFS constant C.

In 2003, Gerginov *et al.* measured the hyperfine splittings of the $6p_{3/2}$ state of Cs with an accuracy of about 2 kHz and determined the C constant [9]. The influence of second-order effects on the hyperfine structure constants was also evaluated [9,10]. From 2018 to 2022, high-precision measurements of hyperfine splittings of other four states $8p_{3/2}$ [11], $6d_{3/2}$ [12], $7d_{3/2}$ [13], and $7d_{5/2}$ [14] had also been reported, and the corresponding HFS constants A, B, and C had been determined using the first-order hyperfine interaction (HFI) theory. However, for experiments with such high precision, the interpretation of measured results may require a more elaborate theoretical investigation. Since the calculation precision of

each state is different, when extracting the HFS constants of these states, it is necessary to evaluate the second-order effect caused by the off-diagonal HFI to see whether the second-order effect brings "correction" to the first-order HFS constants. These analyses also have important guiding significance for future high-precision experiments.

In the present work, we evaluate the first- and second-order HFS constants for the $6p_{3/2}$, $8p_{3/2}$, $6d_{3/2}$, $7d_{3/2}$, and $7d_{5/2}$ states of ^{133}Cs by the relativistic coupled-cluster method. Based on our theoretical calculations, the experimental measurements are reanalyzed and the second-order magnetic dipole–magnetic dipole ($M1$-$M1$) and magnetic dipole–electric quadrupole ($M1$-$E2$) effects on the first-order HFS constant are evaluated. The paper is organized as follows. In Sec. II, we provide a brief overview of the hyperfine structure theory and compile the HFS expressions for the first-order HFS constants of Cs involving the second-order HFI. In Sec. III, we calculate and analyze the modification of the first-order HFS constants due to the second-order effects and present numerical results. Finally, a summary is given in Sec. IV. Atomic units (a.u.) are used unless otherwise stated.

II. THEORETICAL METHOD

A. The hyperfine interaction

Compared with fine structure splitting, hyperfine splitting is much smaller, so the hyperfine interaction may be treated as a perturbation. The hyperfine interaction Hamiltonian for a relativistic electron can be expressed as [1,15]

$$H_{\text{HFI}} = \sum_k T^{(k)} \cdot M^{(k)}, \qquad (1)$$

where $T^{(k)}$ and $M^{(k)}$ are the spherical tensor operators of rank k ($k > 0$) in the electronic and nuclear coordinate spaces, respectively. The matrix element between two hyperfine states

---
*tangyongbo@sztu.edu.cn

can be calculated according to

$$E_F^{\text{HFS}} = \langle \gamma' IJ'F'M_F'|H_{\text{HFI}}|\gamma IJFM_F\rangle = \delta_{F'F}\delta_{M_F'M_F}(-1)^{I+J+F}\sum_k \begin{Bmatrix} F & J & I \\ k & I & J' \end{Bmatrix}\langle\gamma'J'\|T^{(k)}\|\gamma J\rangle\langle I\|M^{(k)}\|I\rangle, \tag{2}$$

where $\mathbf{I}$, $\mathbf{J}$, and $\mathbf{F}$ are the nuclear, atomic, and total angular momentum, and $|\gamma IJFM_F\rangle$ is the hyperfine state constructed from coupling a nuclear eigenstate $|IM_I\rangle$ with an atomic eigenstate $|\gamma JM_J\rangle$ with γ representing the remaining electronic quantum numbers. The first-order correction $E_F^{(1)}$ of HFI to the energy can thus be defined as

$$E_F^{(1)} = (-1)^{I+J+F}\sum_k \begin{Bmatrix} F & J & I \\ k & I & J \end{Bmatrix}\langle\gamma J\|T^{(k)}\|\gamma J\rangle\langle I\|M^{(k)}\|I\rangle. \tag{3}$$

The nuclear matrix elements are given in terms of conventional nuclear moments through

$$\langle II|M^{(1)}|II\rangle = \mu, \tag{4}$$

$$\langle II|M^{(2)}|II\rangle = \tfrac{1}{2}Q, \tag{5}$$

$$\langle II|M^{(3)}|II\rangle = -\Omega, \tag{6}$$

where μ is the nuclear magnetic dipole moment, Q is the nuclear electric quadrupole moment, and Ω is the nuclear magnetic octupole moment. Restricted to $k \leqslant 3$, $E_F^{(1)}$ in Eq. (3) can be parameterized in terms of the magnetic dipole ($M1$), electric quadrupole ($E2$), and magnetic octupole ($M3$) HFS constants A, B, and C according to

$$A = \frac{\mu}{I}\frac{\langle\gamma J\|T^{(1)}\|\gamma J\rangle}{\sqrt{J(J+1)(2J+1)}}, \tag{7}$$

$$B = 2Q\left[\frac{2J(2J-1)}{(2J+1)(2J+2)(2J+3)}\right]^{1/2}\langle\gamma J\|T^{(2)}\|\gamma J\rangle, \tag{8}$$

$$C = \Omega\left[\frac{J(2J-1)(J-1)}{(J+1)(J+2)(2J+1)(2J+3)}\right]^{1/2}\langle\gamma J\|T^{(3)}\|\gamma J\rangle. \tag{9}$$

Then the second-order correction $E_F^{(2)}$ of hyperfine interaction to the energy is defined as [16]

$$E_F^{(2)} = \sum_{\gamma J'}\sum_{k_1,k_2}\frac{\langle(\gamma IJ')FM_F|T^{(k_1)}\cdot M^{(k_1)}|(\gamma IJ)FM_F\rangle}{E_{\gamma J}-E_{\gamma' J'}}\langle(\gamma IJ')FM_F|T^{(k_2)}\cdot M^{(k_2)}|(\gamma IJ)FM_F\rangle$$

$$\approx \underbrace{\sum_{J'}\left|\begin{Bmatrix} F & J & I \\ k_1 & I & J' \end{Bmatrix}\right|^2\eta}_{M1-M1:\,k_1=k_2=1} + \underbrace{\sum_{J'}\begin{Bmatrix} F & J & I \\ k_1 & I & J' \end{Bmatrix}\begin{Bmatrix} F & J & I \\ k_2 & I & J' \end{Bmatrix}\zeta}_{M1-E2:\,k_1=1,k_2=2}, \tag{10}$$

where

$$\eta = \frac{(I+1)(2I+1)}{I}\mu^2\frac{|\langle\gamma J'\|T^{(1)}\|\gamma J\rangle|^2}{E_{\gamma J}-E_{\gamma J'}}, \tag{11}$$

$$\zeta = \frac{(I+1)(2I+1)}{I}\sqrt{\frac{2I+3}{2I-1}}\mu Q\frac{\langle\gamma J'\|T^{(1)}\|\gamma J\rangle\langle\gamma J'\|T^{(2)}\|\gamma J\rangle}{E_{\gamma J}-E_{\gamma J'}}. \tag{12}$$

In the above, the summation involves all possible excited electronic states, and $\langle\gamma'J'\|T^{(k)}\|\gamma J\rangle$ is the reduced matrix element of the electronic part. Here we focus on $M1$ and $E2$ off-diagonal reduced matrix elements between two nearby fine-structure levels, i.e., $J' = J \pm 1$, because these contributions dominate owing to small energy denominators.

The single-particle reduced matrix elements of the operators $T^{(1)}$, $T^{(2)}$, and $T^{(3)}$ are given by

$$\langle\kappa_v\|T^{(1)}\|\kappa_w\rangle = -\langle-\kappa_v\|C^{(1)}\|\kappa_w\rangle(\kappa_v+\kappa_w)\int_0^\infty dr\frac{P_v(r)Q_w(r)+P_w(r)Q_v(r)}{r^2}, \tag{13}$$

$$\langle\kappa_v\|T^{(2)}\|\kappa_w\rangle = -\langle\kappa_v\|C^{(2)}\|\kappa_w\rangle\int_0^\infty dr\frac{P_v(r)P_w(r)+Q_v(r)Q_w(r)}{r^3}, \tag{14}$$

TABLE I. The parameters of the Gaussian basis set, where N is the size of basis set for each symmetry, and N_c and N_v represent, respectively, the numbers of core and virtual orbitals.

	s	p	d	f	g	h	i
$\alpha \times 10^3$	0.725	0.525	0.570	86	86	86	86
β	1.85	1.85	1.90	2.1	2.1	2.1	2.1
N	40	40	40	25	20	15	10
N_c	6	5	3	1	1	1	1
N_v	29	28	27	17	17	15	10

and

$$\langle \kappa_v \| T^{(3)} \| \kappa_w \rangle = -\frac{1}{3} \langle -\kappa_v \| C^{(3)} \| \kappa_w \rangle (\kappa_v + \kappa_w)$$
$$\times \int_0^\infty dr \frac{P_v(r)Q_w(r) + P_w(r)Q_v(r)}{r^4}, \quad (15)$$

where the relativistic angular-momentum quantum number $\kappa = \ell(\ell + 1) - j(j + 1) - 1/4$, and P and Q are, respectively, the large and small radial components of the Dirac wave function. The reduced matrix element

$$\langle \kappa_v \| C^{(k)} \| \kappa_w \rangle = (-1)^{j_v + 1/2} \sqrt{(2j_v + 1)(2j_w + 1)}$$
$$\times \begin{Bmatrix} j_v & k & j_w \\ 1/2 & 0 & -1/2 \end{Bmatrix} \pi(\ell_v, k, \ell_w) \quad (16)$$

satisfies the condition $\pi(\ell_v, k, \ell_w) = 1$ when $\ell_v + k + \ell_w$ is even; otherwise $\pi(\ell_v, k, \ell_w) = 0$.

We employed a finite basis set, composed of even-tempered Gaussian-type functions expressed as $G_i = \mathcal{N}_i r^{\ell+1} e^{-\alpha_i r^2}$, to expand the Dirac radial wave functions P and Q as in Ref. [17], where $\mathcal{N}_i$ is the normalization factor, and $\alpha_i = \alpha \beta^{i-1}$, with the two independent parameters α and β being optimized separately for each orbital symmetries. Table I lists the Gaussian basis parameters, where N is the size of basis set for each symmetry, and N_c and N_v represent, respectively, the number of core and virtual orbitals.

To accurately calculate the matrix elements in Eqs. (7)–(12), we must determine the wave function of the atomic state, which involves solving the electron correlation problem. In the present work, the correlation effects are investigated using *ab initio* methods at different levels, including the Dirac-Fock (DF) approximation, and linearized and fully single- and double-excitation relativistic coupled-cluster methods, denoted respectively by LCCSD and CCSD. The detailed description of these methods can be found in our previous works for Fr, Ra$^+$, and Th^{3+} in Refs. [18–20]. In practice, the no-pair Dirac Hamiltonian was set as the starting point. The Fermi nuclear distribution was employed to describe the Coulomb potential between electrons and the nucleus. All the core and virtual orbitals with energies of smaller than 10000 a.u. were included in the correlation calculations.

B. Expressions of A, B, and C constants involving second-order HFI

From the previous subsection, we know that to accurately determine the first-order constants A, B, and C from the measured HFS intervals, it is necessary to have
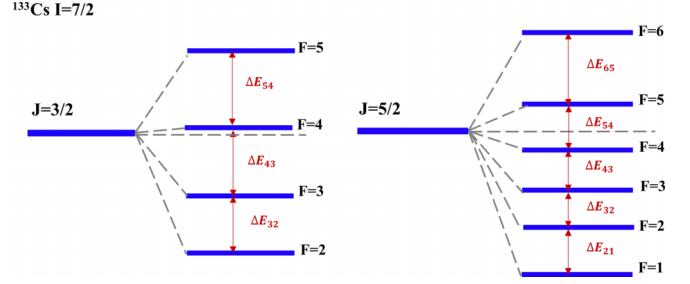

FIG. 1. Schematic diagram of HFS in ^{133}Cs for states of $J = 3/2$ and $J = 5/2$, where $\Delta E_{FF'}$ with $F' = F - 1$ (same as below) denotes the energy difference between two adjacent hyperfine levels determined by experiment; see Table II.

knowledge of higher order effects. If we only consider the $M1$-$M1$ and $M1$-$E2$ second-order interactions described by the second-order constants η and ζ (here we assume all other second- and higher order effects are negligible), the energy level of total quantum number of F can be expressed as $E_F^{\mathrm{HFS}} = E_J + E_F^{(1)}(A, B, C) + E_F^{(2)}(\eta, \zeta)$. Then the hyperfine interval $\Delta E_{FF'} = E_F^{\mathrm{HFS}} - E_{F'}^{\mathrm{HFS}}$ can be written as $\Delta E_{FF'} = \Delta E_{FF'}^{(1)}(A, B, C) + \Delta E_{FF'}^{(2)}(\eta, \zeta)$, which can be determined experimentally. Figure 1 shows the hyperfine structure of ^{133}Cs in the $J = 3/2$ and $J = 5/2$ manifolds. We may solve for A, B, and C in terms of the HFS intervals $\Delta E_{FF'}$, as well as η and ζ. The following expressions are the A, B, and C constants for the states $np_{3/2}$, $nd_{3/2}$, and $nd_{5/2}$.

For the $np_{3/2}$ state,

$$A^{np_{3/2}} = \frac{11}{120} \Delta E_{54} + \frac{2}{21} \Delta E_{43} + \frac{3}{56} \Delta E_{32}$$
$$+ \frac{1}{1512} \eta^{np_{3/2}} - \frac{1}{1260} \zeta^{np_{3/2}}, \quad (17)$$

$$B^{np_{3/2}} = \frac{77}{120} \Delta E_{54} - \frac{1}{3} \Delta E_{43} - \frac{5}{8} \Delta E_{32}$$
$$+ \frac{1}{36} \eta^{np_{3/2}} + \frac{1}{120} \zeta^{np_{3/2}}, \quad (18)$$

$$C^{np_{3/2}} = \frac{7}{480} \Delta E_{54} - \frac{1}{24} \Delta E_{43} + \frac{1}{32} \Delta E_{32}$$
$$+ \frac{1}{480} \zeta^{np_{3/2}}. \quad (19)$$

For the $nd_{3/2}$ state,

$$A^{nd_{3/2}} = \frac{11}{120} \Delta E_{54} + \frac{2}{21} \Delta E_{43} + \frac{3}{56} \Delta E_{32}$$
$$- \frac{1}{2520} \eta^{nd_{3/2}} - \frac{1}{60} \zeta^{nd_{3/2}}, \quad (20)$$

$$B^{nd_{3/2}} = \frac{77}{120} \Delta E_{54} - \frac{1}{3} \Delta E_{43} - \frac{5}{8} \Delta E_{32}$$
$$+ \frac{1}{180} \eta^{nd_{3/2}} - \frac{7}{120} \sqrt{\frac{1}{105}} \zeta^{nd_{3/2}}, \quad (21)$$

$$C^{nd_{3/2}} = \frac{7}{480} \Delta E_{54} - \frac{1}{24} \Delta E_{43} + \frac{1}{32} \Delta E_{32}$$
$$+ \frac{1}{480} \sqrt{\frac{1}{105}} \zeta^{nd_{3/2}}. \quad (22)$$

TABLE II. A summary of the experimental hyperfine splittings (in MHz) for the five states in ^{133}Cs. $\Delta_{JJ'} = E_{\gamma J} - E_{\gamma J'}$ represents the interval between two nearby fine-structure levels, where $J' = J \pm 1$.

Level	ΔE_{65}	ΔE_{54}	ΔE_{43}	ΔE_{32}	ΔE_{21}	Source	$\Delta_{JJ'}$ [21]
$6p_{3/2}$		251.0916(20)	201.2871(11)	151.2247(16)		Ref. [9]	16609672.05
$8p_{3/2}$		38.130(30)	30.242(82)	23.026(38)		Ref. [11]	2478462.54
$6d_{3/2}$		81.615(30)	65.335(14)	49.164(24)		Ref. [12]	−1285069.55
$7d_{3/2}$		36.725(6)	29.415(6)	22.082(7)		Ref. [13]	−627729.52
$7d_{5/2}$	−10.225(9)	−8.542(7)	−6.849(7)	−5.134(29)	−3.320(7)	Ref. [14]	627729.52

For the $nd_{5/2}$ state,

$$A^{nd_{5/2}} = \frac{61}{1320}\Delta E_{65} + \frac{267}{3080}\Delta E_{54} + \frac{9}{280}\Delta E_{43} + \frac{9}{280}\Delta E_{32}$$
$$+ \frac{9}{280}\Delta E_{21} + \frac{1}{3780}\eta^{nd_{5/2}} - \frac{1}{210}\sqrt{\frac{1}{105}}\zeta^{nd_{5/2}}, \quad (23)$$

$$B^{nd_{5/2}} = \frac{245}{264}\Delta E_{65} + \frac{1}{88}\Delta E_{54} - \frac{5}{8}\Delta E_{43} - \frac{5}{8}\Delta E_{32}$$
$$- \frac{5}{8}\Delta E_{21} + \frac{1}{54}\eta^{nd_{5/2}} + \frac{1}{12}\sqrt{\frac{1}{105}}\zeta^{nd_{5/2}}, \quad (24)$$

$$C^{nd_{5/2}} = -\frac{21}{352}\Delta E_{65} + \frac{45}{352}\Delta E_{54} - \frac{11}{352}\Delta E_{43} - \frac{11}{352}\Delta E_{32}$$
$$- \frac{11}{352}\Delta E_{21} + \frac{1}{48}\sqrt{\frac{1}{105}}\zeta^{nd_{5/2}}. \quad (25)$$

In the above Eqs. (17)–(25), all the required $\Delta E_{FF'}$ from Refs. [9,11–14] are summarized in Table II, where $\Delta_{JJ'}$ represents the interval between two nearby fine-structure levels obtained from Ref. [21].

III. RESULTS AND DISCUSSION

It can be seen from Eqs. (17)–(25) that the second-order HFS constants η and ζ need to be evaluated using atomic structure theory in order to accurately extract the first-order HFS constants A, B, and C. Since the diagonal hyperfine matrix elements of the first-order HFS constants in Eqs. (7)–(9) and the off-diagonal hyperfine matrix elements of the second-order HFS constants in Eqs. (11) and (12) are obtained simultaneously, we calculated the first-order HFS constants A and B and compared the results with the experimental values to verify the reliability of our calculation before evaluating the second-order HFS constants η and ζ. In addition, the magnetic octupole hyperfine-interaction diagonal matrix elements are also calculated in this work, and combined with the reported C constants, the magnetic octupole moment of ^{133}Cs is analyzed. The magnetic dipole moment μ is taken from Ref. [22] as $2.5827681(14)\mu_N$, and the electric quadrupole moment Q is taken from Ref. [9] as $-0.00355(4)$ b.

A. First-order HFS constant A

The HFS constants A of ^{133}Cs at different correlation levels, including DF, LCCSD, and full CCSD calculations, are tabulated in Table III, where the CCSD results are our

TABLE III. The HFS constant A (MHz) of ^{133}Cs at different correlation levels: DF, LCCSD, and CCSD, where the CCSD results are our recommended values with percentage uncertainty "Unc.%" due to higher order correlation effect beyond the CCSD method. Other theoretical and experimental values are also listed for comparison.

	A_{present}				A_{other}				
	DF	LCCSD	CCSD	Unc.%	Theory		Experiment		
$6p_{1/2}$	160.32	310.25	292.16	6.2	291.49 [23]	289.6 [24]	291.9309(12) [25]	291.9135(15) [26]	291.929(1) [27]
					290.41 [6]	289.655 [28]	291.918(8) [29]	291.922(20) [30]	291.885(80) [31]
$6p_{3/2}$	23.86	51.85	49.53	4.7	47.6 [9]	48.51 [24]	**50.28827(23)** [9]	50.28163(86) [32]	50.275(3) [33]
$8p_{1/2}$	26.98	44.28	42.51	4.2	42.32 [6]	42.43 [24]	**42.933(8)** [11]	42.95(25) [34]	42.92(25) [35]
					42.95(9)[a]	42.93(7)[b]	42.97(10) [36]		
$8p_{3/2}$	4.07	7.58	7.40	2.5	7.44 [6]	7.27 [24]	**7.609(8)** [11]	7.42(6) [37]	7.644(25) [38]
							7.626(5) [39]	7.58(1) [40]	
$6d_{3/2}$	9.30	17.61	16.76	5.1	16.93 [6]	17.80 [41]	**16.338(3)** [12]	16.34(3) [42]	16.17(17) [43]
$6d_{5/2}$	3.58	−3.87	−3.43	13	−3.48 [6]	−3.89 [41]	**−4.629(14)** [44]	−4.59(6) [45]	−4.66(4) [42]
							−4.56(9) [43]	−4.69(4) [46]	
$7d_{3/2}$	4.71	7.79	7.42	5.0	7.48 [6]	7.88 [41]	**7.3509(9)** [13]	7.386(15) [47]	7.38(1) [48]
							7.36(3) [49]	7.36(7) [50]	7.39(6) [51]
$7d_{5/2}$	1.89	−1.43	−1.26	13	−1.13 [6]	−1.42 [41]	**−1.70867(62)** [14]	−1.717(15) [47]	−1.81(5) [50]
							−1.79(5) [51]		

[a] Ref. [52], a fitting method by Grunefeld *et al.*
[b] Ref. [52], a ratio method by Grunefeld *et al.*

TABLE IV. The HFS constant B (MHz) of ^{133}Cs at different correlation levels: DF, LCCSD, and CCSD, where the CCSD results are our recommended values with percentage uncertainty "Unc.%" due to higher-order correlation effect beyond the CCSD method. Other theoretical and experimental values are also listed here for comparison.

	$B_{present}$				B_{other}			
	DF	LCCSD	CCSD	Unc.%	Theory		Experiment	
$6p_{3/2}$	−0.2226	−0.5177	−0.4901	5.6	−0.5041[a], −0.4935[b]	**−0.4940(17)**[9]	−0.5266(57)[32]	−0.53(2)[33]
$8p_{3/2}$	−0.0380	−0.0729	−0.0701	3.9		**−0.005(40)**[11]	−0.090(24)[39]	−0.049(42)[53]
						−0.14(5)[40]		
$6d_{3/2}$	−0.0290	−0.0583	−0.0569	2.5		**−0.136(24)**[12]	−0.36(1)[54]	−0.1(2)[42]
						0.11(127)[43]		
$6d_{5/2}$	−0.0374	−0.0793	−0.0775	2.6		−0.10(15)[44]	−0.78(66)[45]	0.9(8)[42]
						−0.35(183)[43]	0.18(73)[46]	
$7d_{3/2}$	−0.0147	−0.0258	−0.0249	3.5		**−0.041(8)**[13]	−0.18(16)[47]	−0.18(10)[48]
						−0.1(2)[49]	−0.88(87)[50]	−0.19(18)[51]
$7d_{5/2}$	−0.0188	−0.0351	−0.0339	3.6		**−0.050(14)**[14]	−0.18(52)[47]	1.10(106)[50]
						1.05(29)[51]		

[a]Ref. [9], 142Q, semiempirical estimation by Gerginov *et al*.
[b]Ref. [9], 139Q, MBPT calculation by Gerginov *et al*.

recommended values with percentage uncertainty "Unc.% " mainly from higher order correlation effect beyond the CCSD method. The uncertainty may be assumed to be not greater than the contribution of the lower-order non-linear terms, i.e., CCSD − LCCSD, or 5% of the total electron correlation, i.e., (CCSD − DF) × 5%. Therefore, to be more conservative, we take the greater between |(CCSD − LCCSD)/CCSD| and |(CCSD − DF)/CCSD × 5%| as the uncertainty. Other theoretical [6,9,23,24,28,39,41,52] and experimental [9,11,12,14,25–27,29–38,40,42,42–45,47,49–51] values are also listed in the table to compare with our CCSD results, with particular attention on those in bold.

One can see from Table III the importance of correlation effect in calculating A. For the $p_{1/2,3/2}$ and $d_{3/2}$ states, the total electron correlation effect is nearly half of the CCSD result. For the $6d_{5/2}$ and $7d_{5/2}$ states, the inclusion of correlation effect by CCSD improves the DF values by 210% and 250%, respectively, regardless of the sign, which suggests that the correlation effect plays a significant role in $d_{5/2}$. Moreover, the opposite sign between CCSD and DF values of $d_{5/2}$ reveals a strong cancellation among different correlation effects.

Our CCSD values are also compared with other theoretical and experimental results. One can see that, except for $d_{5/2}$, our values are in agreement with other *ab initio* theoretical results [6,9,23,24,28,39,41,52], and the differences from experimental results are within 3%, which do not exceed our estimated uncertainties. For $d_{5/2}$, the difference between our theory and experiment is about 26%, indicating the importance of higher order correlation effects not included here.

B. First-order HFS constant B

Similar to the case of A constant, the B constant is also calculated and listed in Table IV, where the total electron correlation effect is nearly half of the CCSD, and the uncertainty in CCSD is less than 6%. There are very few theoretical results for B, only the $6p_{3/2}$ state has been reported. For $6p_{3/2}$, our CCSD result is in good agreement with the calculation of Gerginov *et al*. [9], and also with experimental

values [9,32,33]. Except for the $6p_{3/2}$ state, the differences between the CCSD results and the experimental results are much larger than the estimated uncertainties, and we also find that the differences between the results of different experimental measurements are quite significant, even reflected in the magnitude and sign. This may be caused by the following reasons: (i) The value of the electric quadrupole moment Q we used was determined in Ref. [9] by comparing the B constant of the $6p_{3/2}$ state measured experimentally with the coupling coefficient calculated by the third-order MBPT calculation. However, due to the different measurement accuracy for each state, this Q value may not be accurate for other states, leading to differences between our calculated results and the experimental values. From another point of view, since the CCSD result of $6p_{3/2}$ state is consistent with the experimental values within uncertainty, it implies that the present CCSD calculation is consistent with the third-order MBPT theory in Ref. [9]. (ii) Because the electric quadrupole moment Q is very small, $\approx 10^{-3}$ b, the B constant is very small and so it is difficult accurately measured experimentally, which is why the uncertainties of the experimental values are very large. It is thus understandable that the measured results differ significantly. (iii) The higher order electron correlation effects beyond the CCSD method may also be one of the reasons for the discrepancy between the calculated and measured values.

C. Magnetic octupole hyperfine interaction

Table V lists the magnetic octupole hyperfine-interaction diagonal matrix elements from DF, LCCSD, and CCSD calculations in $\mu_N \times b$. The uncertainties of these octupole parameters are similar to the case of A and B constants. By comparing the results of DF and CCSD, it is found that the magnetic octupole hyperfine interaction is sensitive to the electron correlation effect. For the $6p_{3/2}$, $8p_{3/2}$, $6d_{3/2}$, and $7d_{3/2}$ states, the electron correlation effects account for nearly half of CCSD results. For the $7d_{5/2}$ state, the inclusion of correlation effects change the result of CCSD from the DF value by 125% regardless of the sign, which suggests that the

TABLE V. The magnetic octupole hyperfine-interaction diagonal matrix elements C/Ω ($\frac{\text{kHz}}{\mu_N \times \text{b}}$) of ^{133}Cs at different correlation levels: DF, LCCSD, and CCSD, where the CCSD results are our recommended values with percentage uncertainty "Unc.%" due to higher order correlation effect beyond the CCSD method. "$C_{\text{Expt.}}$" are measured HFS constant C. $\Omega(\mu_N \times \text{b})$ listed in "present" column is determined by combining the measured $C_{\text{Expt.}}$ and the calculated C/Ω by present CCSD method. Other theoretical values are also listed here for comparison.

	C/Ω ($\frac{\text{kHz}}{\mu_N \times \text{b}}$)				$C_{\text{Expt.}}$	$\Omega(\mu_N \times \text{b})$	
γJ	DF	LCCSD	CCSD	Unc.%	(kHz)	present	other
$6p_{3/2}$	0.4562	0.8959	0.8445	6.1	0.56(7) [9]	0.66	0.82(10) [9]
$8p_{3/2}$	0.0780	0.1315	0.1260	4.4	16(4) [11]	126.98	
$6d_{3/2}$	0.0243	0.0463	0.0456	2.3	4.3(10) [12]	94.30	
$7d_{3/2}$	0.0123	0.0197	0.0195	1.8	$-0.027(530)^{\text{a}}, -1.073(530)^{\text{b}}$	$-1.38^{\text{a}}, -55.03^{\text{b}}$	
$7d_{5/2}$	0.0044	-0.0170	-0.0180	6.2	0.4(14) [14]	-22.22	

[a]The HFS $C=-0.027(530)$ kHz is taken from Ref. [13], combined with the C/Ω calculated in this work, $\Omega=-1.38\ \mu_N \times \text{b}$ is obtained.
[b]The HFS $C=-1.073(530)$ kHz is derived by Eq.(22), where the ΔE are taken from Ref. [13] (as shown in Table VII). The Ω obtained by combining the calculation of this work is $-55.03\ \mu_N \times \text{b}$.

correlation effect plays a significant role in $d_{5/2}$ state. Moreover, the opposite sign of CCSD value and DF value of $7d_{5/2}$ state reveals a strong cancellation from different correlation effects. By comparing the results of LCCSD and CCSD, it can be found that the electron correlation of the nonlinear terms of all states are about 1% to 6%, suggesting that the higher order electron correlation effects are also important.

Based on these CCSD calculations of matrix elements, and combined with the HFS constants C reported in the experiments [9,11–14], we can obtain the nuclear magnetic octupole moment Ω. From Table V, it can be seen that based on the hyperfine structure constants of different states, the derived Ω differ significantly, not only in magnitude but also in sign. For the $6p_{3/2}$ state, we get Ω is $0.66\mu_N \times \text{b}$, which is close to the MBPT result, $0.82(10)\mu_N \times \text{b}$, reported in the Ref. [9]; the two results are close. For other states, the Ω obtained are extremely large. It is worth noting that for the $7d_{3/2}$ state, the Ω obtained by combining the C constant reported in Ref. [13] with our matrix element is $-1.38\ \mu_N \times \text{b}$, while $-55.03\mu_N \times \text{b}$ when combined with the C constant derived by Eq. (22) in this work (as shown in Table VII). This shows that the measurement accuracy needs to be further improved. In addition, these reported octupole hyperfine interaction di-

agonal matrix elements can provide reference for extracting Ω of ^{133}Cs by more precise experiments in the future.

D. Calculation and analysis of second-order effects

We calculate the off-diagonal hyperfine matrix elements for the five states and evaluate the influence of second-order effects. Table VI shows the results of some off-diagonal hyperfine matrix elements at different correlation levels. "Unc.%" represents the percentage uncertainty due to higher order correlation effect beyond the CCSD method like in the case of A and B constants in Tables III and IV, except for the $|\langle \gamma J' \| T^{(1)} \| \gamma J \rangle|$

TABLE VI. Important off-diagonal matrix elements between two fine-structure states obtained using the DF, LCCSD, and CCSD methods. "Unc.%" represents the percentage uncertainty in CCSD.

γJ	$\gamma J'$	DF	LCCSD	CCSD	Unc.%
		$|\langle \gamma J' \| T^{(1)} \| \gamma J \rangle|$ in MHz/μ_N			
$6p_{3/2}$	$6p_{1/2}$	36.52	34.75	32.00	8.6
$8p_{3/2}$	$8p_{1/2}$	6.19	5.11	4.65	9.9
$6d_{3/2}$	$6d_{5/2}$	-5.85	-105.44	-98.87	35
$7d_{3/2}$	$7d_{5/2}$	-2.95	-43.88	-41.24	35
$7d_{5/2}$	$7d_{3/2}$	2.95	43.88	41.24	35
		$|\langle \gamma J' \| T^{(2)} \| \gamma J \rangle|$ in MHz/b			
$6p_{3/2}$	$6p_{1/2}$	156.48	361.08	341.20	5.8
$8p_{3/2}$	$8p_{1/2}$	26.52	50.26	48.35	4.0
$6d_{3/2}$	$6d_{5/2}$	-11.04	-22.07	-21.60	2.4
$7d_{3/2}$	$7d_{5/2}$	-5.57	-9.78	-9.45	3.5
$7d_{5/2}$	$7d_{3/2}$	5.57	9.78	9.45	7.9

TABLE VII. HFS constants A, B, and C in MHz for the states of $6p_{3/2}$, $8p_{3/2}$, $6d_{3/2}$, $7d_{3/2}$, and $7d_{5/2}$ without and with the second-order corrections. $\sum X_{\Delta E} \times \Delta E$ are the uncorrected A, B, and C values, $X_\eta \times \eta$ are the second-order corrections due to the $M1$-$M1$ HFI, and $X_\zeta \times \zeta$ are the second-order corrections due to the $M1$-$E2$ HFI. [y] denotes the power of 10: 10^y.

HFS	$\sum X_{\Delta E} \times \Delta E$	$X_\eta \times \eta$	$X_\zeta \times \zeta$
	$6p_{3/2}$		
A	50.28825(23)	2.80(45)[−6]	6.35[−8]
B	$-0.4940(17)$	**1.18(19)[−4]**	-6.67[−7]
C	0.00056(7)	0.00	-1.67[−7]
	$8p_{3/2}$		
A	7.609(8)	3.96(40)[−7]	8.77[−9]
B	$-0.005(40)$	1.66(17)[−5]	-9.21[−8]
C	0.016(4)	0.00	-2.30[−8]
	$6d_{3/2}$		
A	16.338(3)	2.07(1.47)[−4]	-3.29[−7]
B	$-0.136(24)$	$-2.90(2.06)[−3]$	-1.15[−6]
C	0.0043(10)	0.00	4.11[−8]
	$7d_{3/2}$		
A	7.3533(9)	7.38(5.24)[−5]	-1.23[−7]
B	$-0.050(8)$	**$-1.03(73)[−3]$**	-4.30[−7]
C	$-0.001073(530)$	0.00	1.54[−8]
	$7d_{5/2}$		
A	$-1.70867(62)$	**4.92(3.49)[−5]**	3.51[−8]
B	0.050(14)	**3.44(2.44)[−3]**	-6.15[−7]
C	0.0004(14)	0.00	-1.54[−7]

of $d_{3/2,5/2}$ states. As can be seen from Table VI, for the $|\langle 6d_{5/2}\|T^{(1)}\|6d_{3/2}\rangle|$ and $|\langle 7d_{5/2}\|T^{(1)}\|7d_{3/2}\rangle|$, the total electron correlation effect and the one represented by the nonlinear term account for about 90% and 6.5% of the corresponding CCSD results, respectively. It is noted that the calculation of diagonal and off-diagonal matrix elements should have a similar level of accuracy. Here we define "$\Delta\%$" as the percentage difference between the CCSD and experimental results relative to CCSD. "$\Delta\%$" of A for $d_{5/2}$ is 35%, which is much greater than the theoretical uncertainty "Unc.%". Here we take the root mean square $\sqrt{(\Delta_{A_{d_{5/2}}}\%)^2 + (\Delta_{A_{d_{3/2}}}\%)^2}$ as the uncertainty of $|\langle\gamma J'\|T^{(1)}\|\gamma J\rangle|$ between $d_{5/2}$ and $d_{3/2}$.

With these off-diagonal hyperfine matrix elements in Table VI, we can calculate the second-order HFS constants, and η and ζ, using Eqs. (11) and (12), where $\Delta JJ'$ can be found in Table II. The expressions of A, B, and C given in Sec. II B can be grouped into three parts: The first part is $\sum X_{\Delta E} \times \Delta E$, which represents A, B, C extracted from experimental measurements based only on the first-order HFI theory, i.e., the uncorrected A, B, C values. The second part is $X_\eta \times \eta$, which represents the correction to the first-order HFS constants due to the second-order $M1$-$M1$ interaction. And the third part is $X_\zeta \times \zeta$, which represents the correction to the first-order HFS constants due to the second-order $M1$-$E2$ interaction, where X represents the coefficients of $\Delta E_{FF'}$, η, or ζ in Eqs. (17)–(25). The calculated results of these three parts are listed in Table VII.

In Table VII, $\sum X_{\Delta E} \times \Delta E$ are the uncorrected A, B, C as mentioned above, and the uncertainties in parentheses are derived from experimental values. However, we find that the $\sum X_{\Delta E} \times \Delta E$ of the five states are the same as those in Refs. [9,11–14], except for the B and C constants of the $7d_{3/2}$ state, where the uncorrected B and C we derived are $-0.050(8)$ MHz and $-0.001073(530)$ MHz, respectively. The corresponding values $-0.041(8)$ MHz and $-0.000027(530)$ MHz are given in Ref. [13], which are obtained from a global fitting to the average HFS equations under different conditions based on the first-order HFI theory. It can also be seen from Table VII that the contribution of the $M1$-$E2$ interaction terms $X_\zeta \times \zeta$ is on the order of mHz to Hz, which can be ignored under the present experimental accuracy. Although the contribution of the $M1$-$M1$ interaction term $X_\eta \times \eta$ is on the order of Hz to kHz, this will lead to corrections for some small HFS constants, which will be discussed next.

For the $6p_{3/2}$ state, the $X_\eta \times \eta$ has an effect on the last digit of B, but it is consistent within the uncertainty. Beloy and

Derevianko calculated the second-order effects of the $6p_{3/2}$ state using the relativistic coupled-cluster method [55] and obtained the corrections (i.e., $X_\eta \times \eta + X_\zeta \times \zeta$ in Table VII) to A, B, and C being 2.38, 97.0, and -0.139 Hz, respectively, which are consistent with our current conclusions. For the $8p_{3/2}$ state, the second-order effect can be ignored under the current measurement accuracy. However, the second-order effect will become important when the experimental accuracy is better than 10 Hz. The $M1$-$M1$ interaction terms result in correction at the last digit of B for the $6d_{3/2}$ and $7d_{3/2,5/2}$ states. Similarly it also results in correction at the last digit of A for the $7d_{5/2}$ state though within the experimental uncertainty.

As can be seen from Table VII, the second-order corrections due to the $M1$-$M1$ HFI on C are zero. For $p_{3/2}$ and $d_{3/2}$ states, the second-order corrections due to the $M1$-$E2$ HFI on C are at the order of Hz. Therefore, when the measurement accuracy reaches the order of Hz, the second-order effect on C needs to be taken into account.

IV. SUMMARY

In this work, the first- and second-order HFS constants of ^{133}Cs are calculated using the RCCSD method. The octupole hyperfine-interaction diagonal matrix elements are also calculated, and it is found that the measurement accuracy of the experiment needs to be further improved in order to accurately extract the Ω of ^{133}Cs. We have demonstrated that the second-order effects cannot simply be neglected in deducing the HFS constants from high-precision measurements of the HFS intervals, especially for the B constant of the $6d_{3/2}$ and $7d_{3/2,5/2}$ states. When the measurement accuracy is further improved by 1–2 orders of magnitude, the accurate extraction of the HFS constants for the $p_{3/2}$ state also needs to take the second-order effects into account. The present calculation can provide a reference for extracting the first-order HFS constants in future high-precision experiments.

[1] C. Schwartz, Phys. Rev. **97**, 380 (1955).

[2] J. Ginges and V. Flambaum, Phys. Rep. **397**, 63 (2004).

[3] B. K. Sahoo, B. P. Das, and H. Spiesberger, Phys. Rev. D **103**, L111303 (2021).

[4] C. S. Wood, S. C. Bennett, D. Cho, B. P. Masterson, J. L. Roberts, C. E. Tanner, and C. E. Wieman, Science **275**, 1759 (1997).

[5] A. Kastberg, B. K. Sahoo, T. Aoki, Y. Sakemi, and B. P. Das, Symmetry **12**, 974 (2020).

[6] Y.-B. Tang, B.-Q. Lou, and T.-Y. Shi, J. Phys. B: At. Mol. Opt. Phys. **52**, 055002 (2019).

[7] J. S. M. Ginges and A. V. Volotka, Phys. Rev. A **98**, 032504 (2018).

[8] M. Allegrini, E. Arimondo, and L. A. Orozco, J. Phys. Chem. Ref. Data **51**, 043102 (2022).

[9] V. Gerginov, A. Derevianko, and C. E. Tanner, Phys. Rev. Lett. **91**, 072501 (2003).

[10] W. R. Johnson, H. C. Ho, C. E. Tanner, and A. Derevianko, Phys. Rev. A **70**, 014501 (2004).

[11] J. A. Quirk, L. Sherman, A. Damitz, C. E. Tanner, and D. S. Elliott, Phys. Rev. A **107**, 012807 (2023).

[12] T.-J. Chen, J.-E. Chen, H.-H. Yu, T.-W. Liu, Y.-F. Hsiao, Y.-C. Chen, M.-S. Chang, and W.-Y. Cheng, Opt. Lett. **43**, 1954 (2018).

[13] B. Rahaman and S. Dutta, Phys. Rev. A **106**, 042811 (2022).

[14] B. Rahaman and S. Dutta, Opt. Lett. **47**, 4612 (2022).

[15] W. R. Johnson, *Atomic Structure Theory: Lectures on Atomic Physics* (Springer, Berlin, 2007)

[16] K. Beloy, A. Derevianko, and W. R. Johnson, Phys. Rev. A **77**, 012512 (2008).

[17] R. K. Chaudhuri, P. K. Panda, and B. P. Das, Phys. Rev. A **59**, 1187 (1999).

[18] B.-Q. Lou, F. Li, P.-Y. Wang, L.-M. Wang, and Y.-B. Tang, Acta Phys. Sin. **68**, 093101 (2019).

[19] F.-C. Li, Y.-B. Tang, H.-X. Qiao, and T.-Y. Shi, J. Phys. B: At. Mol. Opt. Phys. **54**, 145004 (2021).

[20] F.-C. Li, H.-X. Qiao, Y.-B. Tang, and T.-Y. Shi, Phys. Rev. A **104**, 062808 (2021).

[21] A. Kramida, Y. Ralchenko, J. Reader, and NIST ASD Team, NIST Atomic Spectra Database (ver. 5.8), https://physics.nist.gov/asd.

[22] P. Raghavan, At. Data Nucl. Data Tables **42**, 189 (1989).

[23] S. G. Porsev, K. Beloy, and A. Derevianko, Phys. Rev. D **82**, 036008 (2010).

[24] M. S. Safronova, W. R. Johnson, and A. Derevianko, Phys. Rev. A **60**, 4476 (1999).

[25] V. Gerginov, K. Calkins, C. E. Tanner, J. J. McFerran, S. Diddams, A. Bartels, and L. Hollberg, Phys. Rev. A **73**, 032504 (2006).

[26] D. Das and V. Natarajan, J. Phys. B: At. Mol. Opt. Phys. **39**, 2013 (2006).

[27] G. W. Truong, J. D. Anstie, E. F. May, T. M. Stace, and A. N. Luiten, Nat. Commun. **6**, 8345 (2015).

[28] R. Pal, M. S. Safronova, W. R. Johnson, A. Derevianko, and S. G. Porsev, Phys. Rev. A **75**, 042515 (2007).

[29] D. Das, A. Banerjee, S. Barthwal, and V. Natarajan, Eur. Phys. J. D **38**, 545 (2006).

[30] T. Udem, J. Reichert, R. Holzwarth, and T. W. Hänsch, Phys. Rev. Lett. **82**, 3568 (1999).

[31] R. J. Rafac and C. E. Tanner, Phys. Rev. A **56**, 1027 (1997).

[32] D. Das and V. Natarajan, EPL **72**, 740 (2005).

[33] C. E. Tanner and C. Wieman, Phys. Rev. A **38**, 1616 (1988).

[34] Y.-W. Liu and P. E. G. Baird, Appl. Phys. B: Lasers Opt. **71**, 567 (2000).

[35] F. S. Cataliotti, C. Fort, F. S. Pavone, and M. Inguscio, Z. Phys. D: At., Mol. Clusters **38**, 31 (1996).

[36] C. Tai, R. Gupta, and W. Happer, Phys. Rev. A **8**, 1661 (1973).

[37] S. B. Bayram, P. Arndt, O. I. Popov, C. Güney, W. P. Boyle, M. D. Havey, and J. McFarland, Phys. Rev. A **90**, 062510 (2014).

[38] J. Abele, Z. Phys. A **274**, 185 (1975).

[39] S. Rydberg and S. Svanberg, Phys. Scr. **5**, 209 (1972).

[40] A. Faist, E. Geneux, and S. Koide, J. Phys. Soc. Jpn. **19**, 2299 (1964).

[41] M. Auzinsh, K. Bluss, R. Ferber, F. Gahbauer, A. Jarmola, M. S. Safronova, U. I. Safronova, and M. Tamanis, Phys. Rev. A **75**, 022502 (2007).

[42] A. Kortyna, N. A. Masluk, and T. Bragdon, Phys. Rev. A **74**, 022503 (2006).

[43] T. Ohtsuka, N. Nishimiya, T. Fukuda, and M. Suzuki, J. Phys. Soc. Jpn. **74**, 2487 (2005).

[44] M. T. Herd, E. C. Cook, and W. D. Williams, Phys. Rev. A **104**, 042812 (2021).

[45] Z. Wang, J. Zhang, Z. Zeng, K. Yan, H. Zhou, and B. Yang, Laser Optoelectron. Prog. **57**, 030202 (2020).

[46] N. P. Georgiades, E. S. Polzik, and H. J. Kimble, Opt. Lett. **19**, 1474 (1994).

[47] J. E. Stalnaker, V. Mbele, V. Gerginov, T. M. Fortier, S. A. Diddams, L. Hollberg, and C. E. Tanner, Phys. Rev. A **81**, 043840 (2010).

[48] P. V. Kiran Kumar, M. Sankari, and M. V. Suryanarayana, Phys. Rev. A **87**, 012503 (2013).

[49] A. Kortyna, V. Fiore, and J. Farrar, Phys. Rev. A **77**, 062505 (2008).

[50] Y.-C. Lee, Y.-H. Chang, Y.-Y. Chang, Y.-Y. Chen, C.-C. Tsai, and H.-C. Chui, Appl. Phys. B **105**, 391 (2011).

[51] S.-D. Wang, J.-P. Yuan, L.-R. Wang, L.-T. Xiao, and S.-T. Jia, Front. Phys. **16**, 12502 (2021).

[52] S. J. Grunefeld, B. M. Roberts, and J. S. M. Ginges, Phys. Rev. A **100**, 042506 (2019).

[53] H. Bucka and G. von Oppen, Ann. Phys. **465**, 119 (1962).

[54] W.-Y. Cheng, T.-J. Chen, C.-W. Lin, B.-W. Chen, Y.-P. Yang, and H. Y. Hsu, Opt. Express **25**, 2752 (2017).

[55] K. Beloy and A. Derevianko, Phys. Rev. A **78**, 032519 (2008).